Plant Science 253 (2016) 141–153

Contents lists available at ScienceDirect

Plant Science

journal homepage: www.elsevier.com/locate/plantsci

APRF1 promotes flowering under long days in *Arabidopsis thaliana*

Georgios Kapolas[a], Despoina Beris[a], Efthimia Katsareli[a], Pantelis Livanos[a], Aris Zografidis[a], Andreas Roussis[a], Dimitra Milioni[b], Kosmas Haralampidis[a,*]

[a] National and Kapodistrian University of Athens, Faculty of Biology, Department of Botany, 15784 Athens, Greece
[b] Agricultural University of Athens, Department of Agricultural Biotechnology, Iera Odos 75, 11855 Athens, Greece

ARTICLE INFO

Article history:
Received 31 July 2016
Received in revised form
23 September 2016
Accepted 26 September 2016
Available online 29 September 2016

Keywords:
Arabidopsis
Chromatin modification
Flowering
WD40 motif
WDR protein

ABSTRACT

Arabidopsis thaliana flowering time mutants revealed the function of numerous genes that regulate the transition from vegetative to reproductive growth. Analyses of their loci have shown that many of them act as chromatin modifiers. In this study, a combination of molecular and genetic approaches have been implemented, to characterize the function of *APRF1* (*ANTHESIS POMOTING FACTOR 1*) gene in *A. thaliana* and to investigate its role in plant development. *APRF1* encodes for a low molecular weight nuclear WDR protein which displays functional homology to the Swd2 protein, an essential subunit of the yeast histone methylation COMPASS complex. Compared to WT plants, total loss-of-function *aprf1* mutants exhibited shoot apical meristem (SAM) alterations and increased growth rates. However, the vegetative phase of *aprf1* plants was prolonged and bolting was delayed, indicating an impairment in flowering under long days (LD). On the contrary, overexpression of *APRF1* accelerates flowering. Consistent with the late flowering phenotype, the molecular data confirmed that *FLC* and *SOC1* expression were significantly altered in the *aprf1* mutants. Our data suggest that APRF1 acts upstream of *FLC* and promotes flowering under LD.

1. Introduction

Living systems manifest their spatiotemporal organization through complex networks of regulatory interactions. Scaffolding proteins play a crucial role in governing intracellular molecular interactions through the cooperative assembly of protein complexes. Interactome studies suggest that WD-repeat proteins (WDRs) are capable of creating scaffolds, on which protein complexes can be reversibly assembled and protein–protein or protein-DNA interactions can ensue [1–3]. WDRs have a β-propeller architecture that is formed by 4–16 short tandem repeat units, named WD40-motifs, configuring a single or multiple structural WD40 domains [3]. A WD40-motif consists of a 40 amino acid core region including a conserved GH dipeptide in the N-terminus and a signature WD dipeptide in the C-terminus [4].

WDR proteins are widespread in eukaryotes and mediate a variety of regulatory interactions in eukaryotic cells, revealing an ancient or proto-eukaryotic origin [5]. In yeast, the WDR protein Swd2 (COMPASS component SWD2) is essential for viability and was shown to have dual-function, indicating the recruitment of the same protein in the assembly of two distinct complexes. As a bona fide subunit of COMPASS (COMPLEX OF PROTEINS ASSOCIATED WITH Set1) it is involved in lysine 4 methylation of histone H3, whereas as a component of the CPF (CLEAVAGE AND POLYADENYLATION FACTOR) complex it participates in RNAP II transcription termination and 3′ end processing [6–8].

In plants, WDRs protein are members of a superfamily with remarkable functional diversity. They are involved in a broad spectrum of cytoplasmic or nucleoplasmic significant processes, such as transcriptional regulation via chromatin modifications, signal transduction, protein modification via ubiquitination, cell cycle control and cell division [3,9,10]. The proteome of *A. thaliana* contains *c.* 269 WDRs, categorized into 143 distinct families [11]. Many of these proteins are subunits of complexes that regulate diverse developmental processes, including the differentiation of epidermal cells [12], pollen [13] and embryo development [14], meristem organization [15] and adaptation to long day lengths and flowering time control [16,17].

* Corresponding author at: National and Kapodistrian University of Athens, Biology Department, Division of Botany, Molecular Plant Development Laboratory, 1578 Athens, Greece.
E-mail addresses: gkapolas@yahoo.gr (G. Kapolas), debthem@hotmail.com (D. Beris), ekatsa@hotmail.com (E. Katsareli), plivanos@biol.uoa.gr (P. Livanos), aristzo@yahoo.gr (A. Zografidis), aroussis@biol.uoa.gr (A. Roussis), bmbi2mid@aua.gr (D. Milioni), kharalamp@biol.uoa.gr (K. Haralampidis).

http://dx.doi.org/10.1016/j.plantsci.2016.09.015
0168-9452/

Flowering is the process that signifies the developmental turning point from the vegetative to the reproductive phase. The onset of flowering is regulated by at least four flowering pathways: the photoperiod, the gibberellic acid (GA), the autonomous and the vernalization. In the photoperiod pathway, flowering is promoted by *CONSTANS (CO)*, which induces *FLOWERING LOCUS T* (*FT*), while mutations in both delay flowering under long days (LD) [18]. The GA pathway influences the phase transition in the SAM by promoting the expression of *SUPPRESSOR OF OVEREXPRESSION OF CONSTANS 1* (*SOC1*) [19,20]. In *A. thaliana*, the *ga1* mutants are unable to flower under short day (SD) conditions [21]. Similarly, numerous loci have also been functionally classified into the autonomous and vernalization pathway, since mutations in them may accelerate or delay flowering [22]. A key step in both the autonomous and the vernalization pathway is the regulation of *FLOWERING LOCUS C* (*FLC*), which in turn regulates the floral integrator genes *FT* and *SOC1* [23,24]. In the vernalization pathway, expression of *VERNALIZATION1* and *VERNALIZATION2* (*VRN1* and *VRN2*) is required for the stable maintenance of *FLC* repression during development under elevated temperatures [25]. *FLC* encodes for a MADS-domain protein [26], which quantitatively inhibits floral transition [24], while suppression of *FLC* is critical for the developmental tuning of flowering [27]. Although *SOC1* is controlled by the integration signals of many flowering pathways [28,29], its expression is regulated mainly via the autonomous and the vernalization pathway through *FLC* [28,30].

The analysis of many flowering time genes from *A. thaliana* has revealed their importance in regulating the transition from vegetative to reproductive development [31]. However, our understanding of how these protein components are assembled remains unclear. Here we show that APRF1, a low molecular weight nuclear WD40 protein, substitutes the yeast Swd2 subunit of the COMPASS histone methylation complex, indicating that the plant homolog remains functional in yeast. Loss-of-function mutants exhibited enhanced growth rates and altered gene expression pattern of several key flowering regulators, resulting in a late flowering phenotype. We suggest that *APRF1* plays a significant role during plant development, while its involvement in setting the flowering time in *A. thaliana* is postulated.

2. Materials and methods

2.1. Plant material and growth conditions

Arabidopsis thaliana (L.) Heynh. (ecotype Col-0) plants were used in the present study. The *APRF1* T-DNA insertion lines, WiscDsLox345-348I5 and WiscDsLox489-492K11 were obtained from NASC (Nottingham, UK). Seeds were imbibed at 4 °C for 48 h, surface sterilized, and sown under sterile conditions on Murashige and Skoog (MS) medium containing plates. Transgenic plants were selected on plates containing 100 μM of the herbicide BASTA for seven days and were transferred to soil for further development. For phenotypic analysis, seeds were sown directly on soil. All plants were germinated and grown at 22 °C, in 60–70% relative humidity, with 16 h light and 8 h dark photoperiod and illumination of 110 $\mu mol\, m^{-2}\, s^{-1}$ PAR, supplied by cool-white fluorescent tungsten tubes (Osram, Germany).

2.2. Bioinformatic and phylogenetic analysis

The *APRF1* (*At5g14530*) nucleotide and protein sequences were obtained from TAIR (http://www.arabidopsis.org). Protein sequences used for the phylogenetic analysis were collected from NCBI (http://www.ncbi.nlm.nih.gov/pmc/) using the BLASTp software (http://blast.ncbi.nlm.nih.gov/Blast.cgi). Multiple protein alignments were performed using CLUSTALW2 and CLUSTAL Omega software, hosted at EMBL-EBI (http://www.ebi.ac.uk/Tools/msa/). The ExPaSy software suite (http://www.expasy.org/) and the NCBI Databases (http://www.ncbi.nlm.nih.gov/) were used for all routine bioinformatics analyses. WD40-repeats motifs were identified using SMART (http://smart.embl-heidelberg.de/), WDsPdb (http://wu.scbb.pkusz.edu.cn/wdsp/) [32] and the database for Eukaryotic Linear Motif (ELM) at http://elm.eu.org.

The phylogenetic tree was constructed from multiple sequence alignments using the neighbor-joining method of the PHYLIP package, version 3.65 (University of Washington, Seattle, USA). Amino acid distances were calculated according to the Dayhoff PAM matrix or the Protein Parsimony. Both methods produced trees with essentially identical topologies. The statistical significance was tested by analysis of 1000 bootstrap replicates. The final tree was visualized with TreeView software (https://sourceforge.net/projects/jtreeview/) and refined in Adobe Photoshop CC Extended software (Adobe Systems Inc., USA).

2.3. Nucleic acid extraction, cDNA synthesis, and PCR

DNA and total RNA were extracted from plant tissues using the NucleoSpin® Plant II and NucleoSpin® RNA Plant kits, respectively, according to manufacturer's instructions (Macherey Nagel, Germany). Nucleic acids were quantified using NanoDrop 1000 Spectrophotometer (Thermo Scientific, USA).

Mutant genotypes were PCR-verified by using Taq DNA polymerase (Invitrogen, USA) and combinations of T-DNA and gene-specific primers. First-strand cDNA was synthesized by using 1 μg of total RNA as template and PrimeScript Reverse Transcriptase (Takara-Clontech, Japan) or Expand Reverse Transcriptase (Roche Diagnostics Ltd, Germany). PCR products for cloning were amplified with Phusion® High-Fidelity DNA Polymerase (New England Biolabs, USA) or with Expand™ High Fidelity DNA Polymerase (Roche, Germany). For semi-quantitative (sq-) and quantitative (q) RT-PCR, Taq DNA polymerase (Invitrogen, USA) and KAPA SYBR® FAST qPCR Kits (Kapa Biosystems, USA) were used, respectively, according to manufacturer's instructions. Quantitative RT-PCR experiments were conducted in triplicates and the relative quantification method ($2^{-\Delta\Delta Ct}$) was used to evaluate variation between replicates. Data were normalized against the constitutively expressed *AtGAPDH*. PCR products were separated by electrophoresis on 0.8–1.2% agarose gels and purified by using the NucleoSpin Gel or the PCR Clean-up kits (Macherey Nagel, Germany). Gels were stained with ethidium bromide (100 $\mu g\, L^{-1}$) and visualized under UV light. All primers used in this study are listed in Supplementary Table A1.

2.4. Yeast complementation

The degron strain Y40075 (ade2-1; ura3-1; his3-11,15; trp1-1; leu2-3,112; can1-100), containing the "heat-inducible degron cassette" at the N-terminus of the YKL018 w ORF locus (SWD2/SAF37/CPF10 gene), was obtained from EUROSCARF (http://web.uni frankfurt.de./fb15/mikro/euroscraf/index.html) [33]. The *A. thaliana* full-length *APRF1* cDNA was amplified by PCR, using primer pair SpeI*AtAPRF1*F/HindIII*AtAPRF1*R, and cloned into the p416GPD yeast vector under the control of the constitutive glyceraldehyde-3-phosphate dehydrogenase (GPD) promoter. Yeast mutant cells (*swd2*Δ) were transformed with two independently generated constructs (p416*APRF1*a and p416*APRF1*b) or with the empty p416GPD vector (negative control), using standard procedures. Ura+ transformants were selected on glucose SC −Ura plates. After growth at 25 °C on YPDA plates containing 0.1 mM $CuSO_4$, cells were re-suspended in PBS to an optical density of 0.8 at 600 nm [OD_{600}]. Drops containing 10-fold serial dilutions were

spotted on plates under four different conditions: SC Glu or SC Gal at 25 °C or 37 °C. Yeast growth was evaluated after 48–72 h.

2.5. Generation of binary vectors and plant transformation

To investigate the subcellular localization of APRF1, an *YFP*:*APRF1* translational fusion construct was generated. In brief, the e*YFP* coding sequence from plasmid pGII0029 was initially cloned as an XhoI/BamHI fragment into the pYES2 vector, excised as an XbaI/SacI fragment and cloned into the respective sites of the linearized pBI121 binary vector, generating construct pB35Sp:e*YFP*. Subsequently, the full length coding sequence of *APRF1* was PCR-amplified using primer pair AscIe*YFP*:*APRF1*F/NotIe*YFP*:*APRF1*-R and ligated into pB35Sp:e*YFP*, generating construct pB35Sp:e*YFP*:*APRF*1.

For the *APRF1*promoter:*GUS* construct, a 466 bp DNA fragment upstream of the translational start codon of *APRF1* was PCR-amplified from genomic DNA, using primers BamHI*APRF1*pGUS-F and NcoI*APRF1*pGUS-R. The purified amplicon was then inserted into the pCambia1201 BamHI/NcoI sites, upstream of the β-glucuronidase (GUS) gene, generating construct p*CAPRF1*p:GUS.

Overexpression of *APRF1* in transgenic lines was driven by the CaMV 35S promoter, generated with construct pB35Sp:*APRF1*. The full length coding sequence was PCR-amplified using primers XbaI*APRF1*-F and SacI*APRF1*-R, and cloned into the pBI121 XbaI/SacI linearized vector. High fidelity DNA polymerases were used for all PCR amplifications. Constructs were checked for integrity and cloning correctness by restriction enzyme analysis and DNA sequencing.

Agrobacterium tumefaciens strain GV3101 competent cells were transformed with the above constructs, using the freeze-thaw method. Plants, of either wild type (Col-0) or *aprf1-7* and *aprf1-9* mutant genetic backgrounds were used to generate stable transgenic *Arabidopsis* lines via the floral dip method. Transformants were selected on MS plates containing Cefotaxime (200 mg L^{-1}), Hygromycin (20 mg L^{-1}) or Kanamycin (40 mg L^{-1}) and transferred to soil till maturity. T_2 and T_3 offspring were subjected to further segregation analysis on selective plates or were grown directly on soil for phenotypic characterization.

2.6. Western blot immunodetection of APRF1

The predicted molecular weight of APRF1 was confirmed by fusing the *APRF1* cDNA to an N-terminal FLAG sequence. The pBI121-based construct (p35S:c*APRF1*:FLAG) was transformed into *A. tumefaciens* GV3101 cells, which were used to infiltrate *N. benthamiana* leaves. Protein samples were separated by SDS-PAGE and transferred onto nitrocellulose membranes. FLAG-tagged APRF1 fusion protein was detected with a primary anti-FLAG antibody (sc-807) and a secondary goat anti-rabbit IgG antibody (sc-2004), (Santa Cruz Biotechnology, USA). Protein bands were visualized by using the LumiSensor™ Chemiluminescent HRP Substrate Kit (L00221V300, GenScript). A schematic representation of all constructs generated in this study are shown in Supplementary Fig. A1 .

2.7. GUS staining and semi-thin sections of resin embedded plant tissues

In situ histochemical GUS staining was conducted in T2 and T3 offspring of 20 individual transgenic plants carrying the p*CAPRF1*p:*GUS* construct. GUS activity was detected by using 5-bromo-4-chloro-3-indolyl-β-D-glucuronide (X-Gluc) as substrate. Seedlings or dissected tissues were incubated for 2 h at 37 °C in X-Gluc buffer (50 mM sodium phosphate, pH 7.2, 0.5 mM potassium ferrocyanide, 0.5 mM potassium ferricyanide, and 2 mM X-Gluc) and dehydrated in an ethanol series. Samples were then cleared with chloral hydrate (5 g chloral hydrate dissolved in 1 ml 30% glycerol), mounted on slides and observed under a microscope or stereomicroscope.

For semi-thin sections, plants were double-fixed with 3% (v/v) glutaraldehyde and 1% (w/v) OsO_4 in sodium cacodylate buffer pH 7.0. Samples were thereafter dehydrated in an acetone or ethanol series, infiltrated in a graded series of Spurr's resin (Serva, Germany) in propylene oxide and finally embedded in small plastic dishes filled with fresh pure resin. Semi-thin sections of the embedded material were obtained with an LKB ultratome III (LKB Produkter AB, Sweden) and stained with 1% (w/v) toluidine blue in 1% (w/v) borax solution or with 1% (w/v) safranin in water.

2.8. Microscopy

Samples were visualized with a Zeiss Axioplan epifluorescence microscope (Zeiss, Germany), equipped with a Zeiss Axiocam MRc5 digital camera, a differential interference contrast (DIC) optical system and the appropriate filters. In particular, a set with exciter BP450-490 and barrier BP515-595 and a set with exciter BP510-560 and a barrier LP590, were used. Stereoscopic photographs were obtained with a Zeiss Stemi 2000-C stereomicroscope, equipped with Jenoptik ProGres3 digital camera (Jenoptik, Germany). All images were processed with Adobe Photoshop CC (Adobe Systems Inc., USA).

2.9. Measuring of flowering time

Flowering time was measured by either the number of days from sowing seeds on soil until the appearance of the first visible floral bud, or by rosette leaf number. With the latter criterion, rosette leaves produced by the meristem were counted in at least 50 plants for each genetic background at the time of bolting. All experiments were performed in triplicates.

3. Results

3.1. AtAPRF1 *encodes for a highly conserved WD40-repeat-containing protein*

In our previous work, we demonstrated the importance of the low molecular weight WDR protein ULCS1 (UBIQUITIN LIGASE COMPLEX SUBUNIT 1) in plant development [34]. In the *Arabidopsis* genome the most closely related sequence of *ULCS1* is encoded by the gene locus *At5g14530* (named herein *APRF1*). Given the structural similarity of the two proteins, the present work has focused on unraveling the functional role of *APRF1* in *Arabidopsis*. The gene, which is organized in 10 exons and 9 introns (Fig. 1A), encodes for a 330 amino acids protein (Fig. 1B) with a molecular mass of ~37 kD (Fig. 1C). APRF1 is annotated in the databases as a trasnducin/WD40 domain-containing protein with seven WD40 repeats constituting a single β-propeller-like WD40 domain (Fig. 1D). It is a conserved protein, sharing high amino acid identity across the plant kingdom; 97% with *Capsella rubella*, 96% with *Brassica rapa*, 96% with *Arabis alpina*, 84% with *Ricinus communis*, 82% with *Vitis vinifera* and 77% with *Zea mays* and *Oryza sativa* orthologs. It also displays a 29%–39% identity to the WDR82 orthologs from several animal species (Supplementary Fig. A2). Interestingly, APRF1 exhibits also a high degree of sequence similarity (52%) and structural homology with the Swd2 subunit of the yeast COMPASS complex (Supplementary Figs. A2, A3 and Table A2). Given the similarity to Swd2, we performed a comparison of the full length amino acid sequence of APRF1 with orthologs that are annotated to function as subunits of histone methylation complexes. Even though Swd2 and APRF1

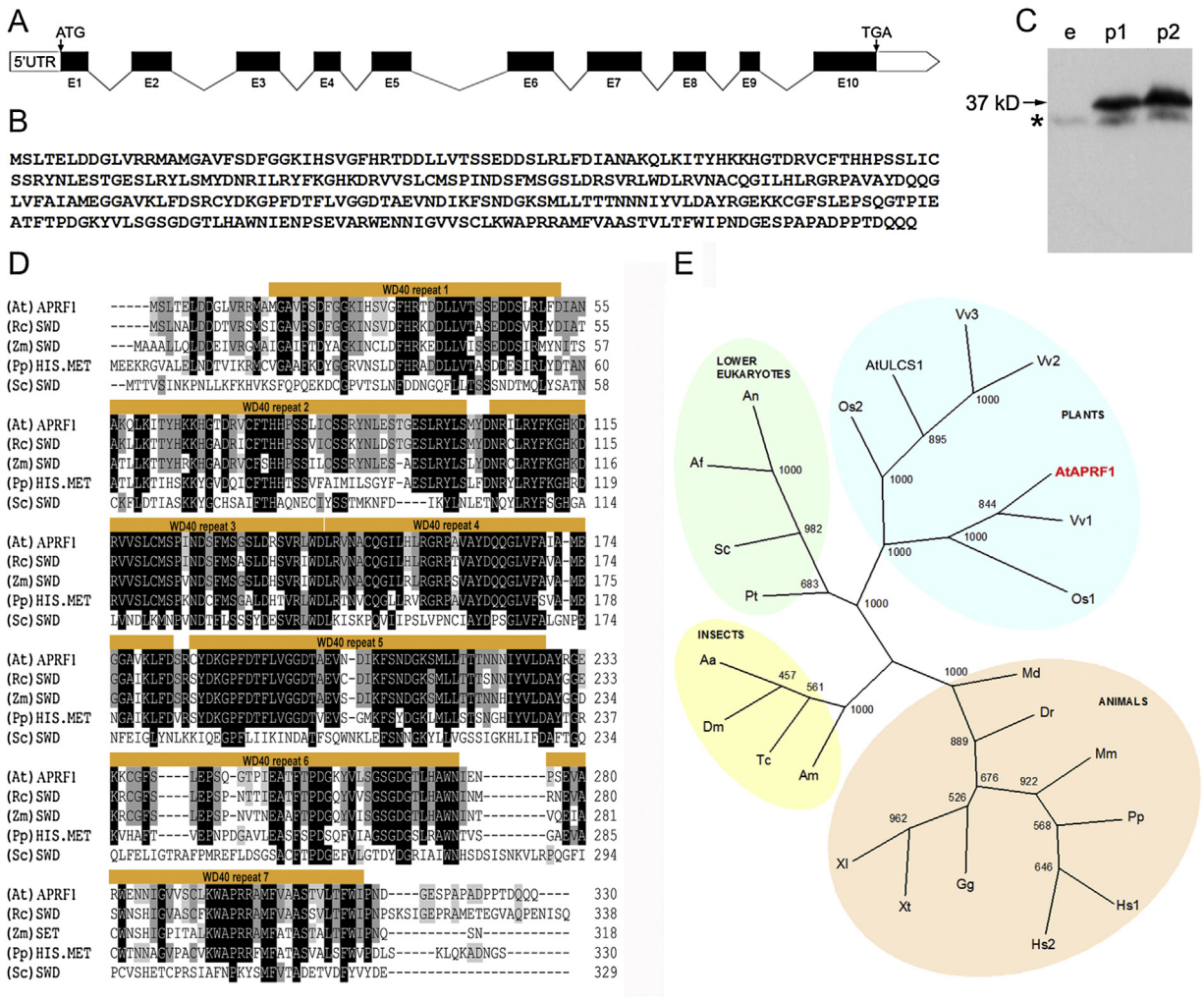

Fig. 1. Bioinformatic and phylogenetic analysis of APRF1. (A) Schematic presentation of the *APRF1* gene structure. (B) APRF1 protein sequence. (C) Western blot showing FLAG tagged APRF1 protein from plants transformed with two independent plasmid constructs (p1 and p2). Arrow refers to the pertinent band. Asterisk indicates nonspecific band. e, control. (D) Alignment of the predicted full-length amino acid sequence of APRF1 with orthologs from organisms that are annotated to function as subunits of histone methylation complexes. Dashes indicate gaps. Numbers indicate total amino acids of each sequence. The distribution of the seven WD40 motifs along the sequence of APRF1 are marked with yellow lines. (E) A consensus bootstrap neighbor-joining tree showing the phylogenetic clustering of APRF1 and other orthologs. The bootstrap scores obtained after 1000 replicates are indicated at the nodes. Abbreviations and the corresponding accession numbers are given in Supplementary Table A3. (For interpretation of the references to colour in this figure legend, the reader is referred to the web version of this article.)

are the most diverged sequences, all proteins shared a high degree of similarity, implying their functional homology (Fig. 1D).

Based on a multiple alignment of the full-length amino acid sequences from different species, a neighbor-joining tree was constructed in order to investigate their phylogenetic relationship (Fig. 1E). The analysis showed an evolutionary partitioning of these WDRs in distinct groups related to their phylogenetic origin. All animal proteins are clustered together into a separate clade, while the yeast Swd2 protein is grouped within the clade formed by the lower eukaryotic sequences. In contrast to animals, plant genomes contain two closely related sequences. Accordingly, APRF1 and the recently characterized ULCS1 homolog [34] from *Arabidopsis* are clustered with high degree of reliability in different branches within the plant clade (Fig. 1E).

3.2. *APRF1 is expressed in aerial parts and the central cylinder of roots*

Semi-quantitative RT-PCR analysis was employed, in order to investigate the expression pattern of *APRF1*. Total RNA was extracted from *Arabidopsis* whole seedlings and root tissues at different developmental stages. *APRF1* was strongly expressed throughout seedling development, whereas in roots the highest expression was observed at 7 days after sowing (Fig. 2A).

To further inspect in detail the tissue-specific expression of *APRF1*, *A. thaliana* transgenic plants harboring an *APRF1*promoter:GUS transcriptional fusion construct were generated (Supplementary Fig. A1). The analysis of GUS reporter activity in independent transgenic lines revealed a temporal and spatial expression pattern of *APRF1* (Fig. 2B–O). During seed development, prominent GUS staining was observed in the endosperm and the developing embryo (Fig. 2B). Following germination, *APRF1* was strongly expressed in the aerial part of the seedlings (Fig. 2C). Intense signal was detected in cotyledons, including the vascular system, the hydathodes and the trichomes, as well as in young leaves and the incipient leaf primordia (Fig. 2D). Significant GUS activity was also observed in the central cylinder of roots and the lower hypocotyl area (Fig. 2C and J). *APRF1* was not expressed in the upper part of the hypocotyl, the primary root tip (including the elongation zone) and the lateral root primordia (Fig. 2C, I and J). GUS staining examination in longitudinal semi-thin sections of seven to twenty-day-old seedlings, confirmed its expression in the

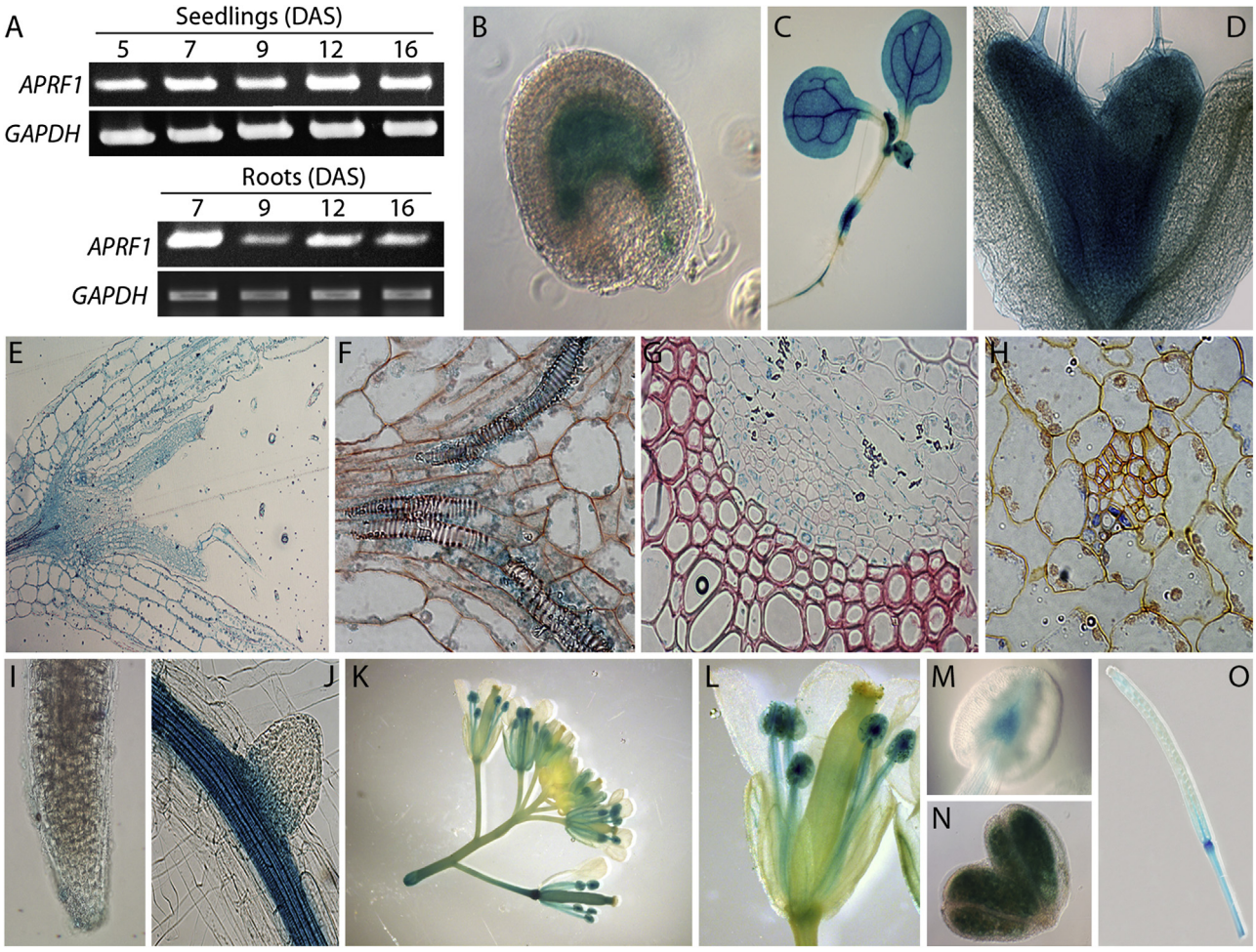

Fig. 2. Expression pattern of *APRF1* during development. (A) Semi-quantitative RT-PCR analysis showing the expression of *APRF1* in 5, 7, 9, 12 and 16 day-old plants and in roots at 7, 9, 12 and 16 days after sowing (DAS). Expression of *GAPDH* was monitored as control. (B–O) Histochemical localization of *APRF1* promoter: *GUS* expression during development. Images showing a representative GUS staining pattern in progeny from line p*CAPRF1*p:GUS T2L21. Similar staining was observed in the majority of independent GUS transgenic lines. *APRF1* was preferentially expressed in the endosperm and developing embryo (B), the cotyledons (C), the juvenile leaves, as well as the trichomes and trichome progenitors cells (C and D). Longitudinal semi-thin sections of seven to twenty DAS seedlings, showing GUS activity in the xylem parenchyma and phloem of the vascular system (E–H). Staining was not detected in root apices and the lateral root primordia (I and J). During the reproductive phase, *APRF1* was strongly expressed in flowers of stages 13–15, predominantly in anthers (K–N). After fertilization, GUS expression was detected in the placenta and the abscission zone of the siliques (O).

SAM and the xylem parenchyma and phloem of the vascular system (Fig. 2E–H).

APRF1 displayed also a specialized expression pattern during reproductive development. Strong GUS activity was observed in flowers of stages 13–15, predominantly in the male reproductive tissues. Staining was prominent in the developing pollen grains, the anther tissues and the filaments. Less expression was detected in the vascular system of sepals and the gynoecium, whereas petals showed negligible GUS staining. After fertilization, *APRF1* was found to be expressed mainly in the placenta and the abscission zone of the siliques (Fig. 2K–O).

3.3. *APRF1 loss-of-function results in spatiotemporal growth alterations*

To evaluate the functional importance of APRF1 in plant development, two independent T-DNA transgenic lines (WiscDsLox345-348I5 and WiscDsLox489-492K11) were obtained from the *Arabidopsis* seed banks. Based on the information provided by TAIR and SALK, the T-DNA insertions were mapped within the 9th intron and 9th exon of the *APRF1* gene (Fig. 3A). Progeny plants of both lines were subjected to segregation analysis and their DNA was used to verify the T-DNA insertion loci (Fig. 3B). Homozygous mutants were selected (*aprf1-7* and *aprf1-9*) and used in further experiments (Fig. 3C). In consistency with the *GUS* reporter gene expression analysis, semi-quantitative RT-PCR analysis revealed that *APRF1* was strongly expressed in all tissues tested, whereas the highest mRNA levels were observed in leaves and flowers. On the contrary, *APRF1* transcripts were not detectable in the *aprf1-7* and *aprf1-9* homozygous lines (Fig. 3C).

Phenotypic analysis of both alleles grown on soil showed that *APRF1* mRNA depletion enhanced the vegetative growth of the plants (Fig. 3D) and delayed flowering (reviewed in section 3.4). In *Arabidopsis*, the aerial architecture of the stem, including lateral branching, is established before primary stem bolting [35]. *APRF1* impaired plants developed faster and exhibited vegetative growth alterations. In both mutants, rosette leaves had extended petioles and a quite undulating surface, compared to WT. They became larger, more elongated and they displayed a slight increase in serration depth, while their margins rolled inward, towards the midrib on the underside (Fig. 3D–E). Due to the prolonged vegetative phase, mutant plants displayed at the initiation of their reproductive phase large rosettes with numerous leaves and flower buds (Fig. 3F). At 50 days after sowing (DAS), *aprf1* mutants possessed *c.* 32 leaves, which was twice the number that are normally developed in WT plants (Fig. 3E). A closer examination, however, revealed that

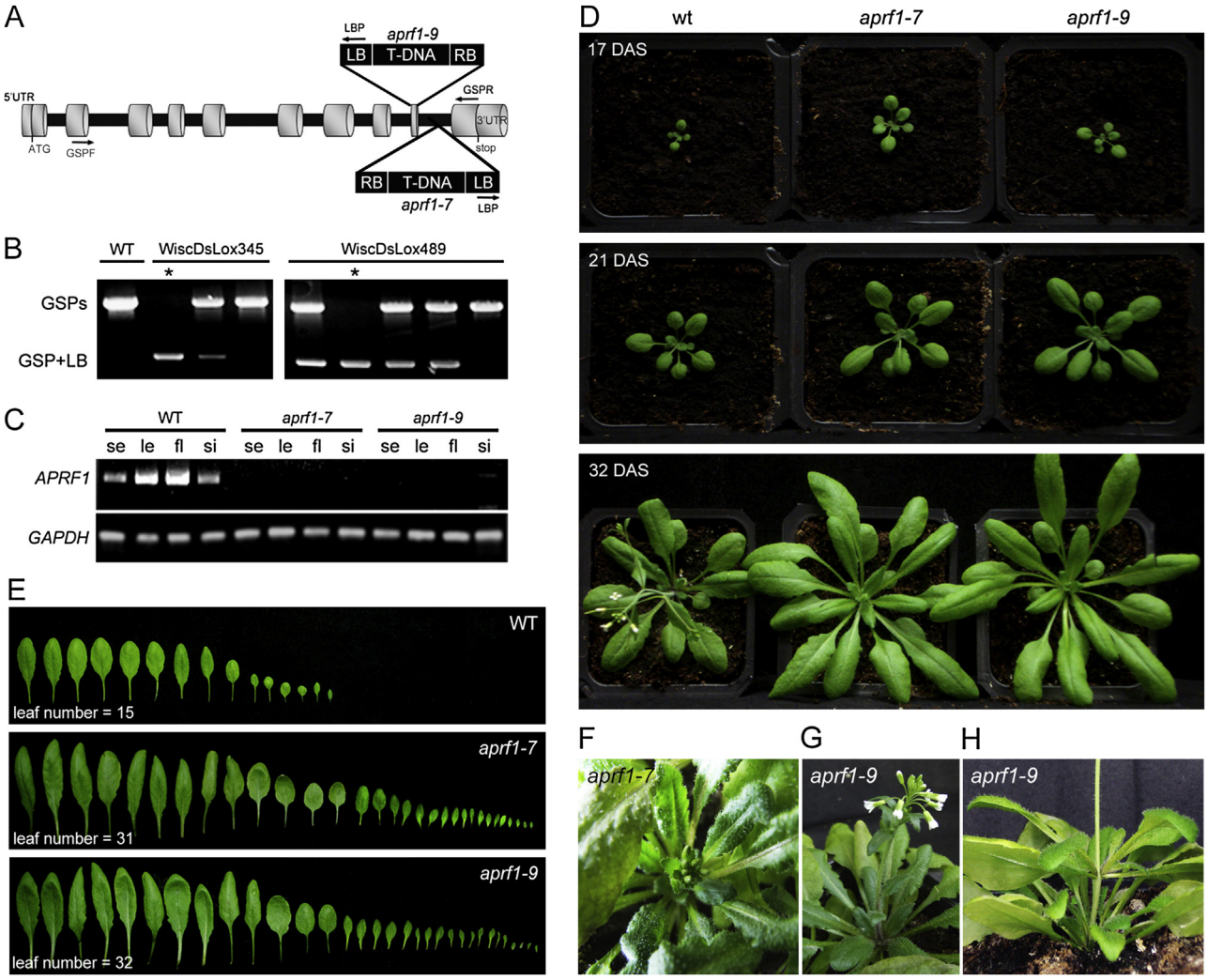

Fig. 3. *APRF1* T-DNA insertion lines and phenotypes. (A) *APRF1* genomic organization and location of T-DNA insertions. Exons and untranslated regions are in grey and introns in black. Location of T-DNA insertions and the primers used for screening (LBP, GSPF, GSPR) are indicated. (B) Verification of the T-DNA insertion by PCR on genomic DNA isolated from WT plants and insertion lines. Asterisks indicate the identified homozygous plants from WiscDsLox345 and WiscDsLox489, named *aprf1-7* and *aprf1-9*, respectively. GSPs, gene specific primers; LB, T-DNA left border primer. (C) RT-PCR showing expression of *APRF1* in WT and absence of the corresponding transcripts in *aprf1-7* and *aprf1-9* homozygous mutants. Expression of *GAPDH* was monitored as control. se, 9 DAS seedlings; le, leaves; fl, flowers; si, siliques. (E) Comparative depiction of the size, shape and number of leaves developed in WT, *aprf1-7 and aprf1-9* plants, when 50% of flowers to be produced have opened (35 DAS, 47 DAS and 52 DAS, respectively). Images showing bolting of *aprf1-7* and *aprf1*-9 plants (F and G) and secondary aerial rosette formed on the primary shoot of *aprf1*-9 (H).

the juvenile leaves surrounding the primary inflorescence were cauline leaves, which were formed during the prolonged vegetative phase (Fig. 3F). This became obvious several days later, by the emergence of a cauline leaf zone with up to nine leaf/paraclades on the protruding primary inflorescence stem (Fig. 3G, see also Fig. 4). In a few cases, a secondary aerial rosette was observed on the primary shoot of mutant plants (Fig. 3H). Models for the development of aerial rosettes assume that these vegetative structures are formed by axillary meristems that are insensitive to inflorescence transition signals [36].

3.4. *aprf1 mutants are delayed in flowering*

Flowering begins with floral transition that leads to the emergence of the first flower, followed by bolting transition that is characterized by the elongation of the first internode [35]. As these developmental transitions are under the influence of various endogenous and exogenous factors, plants were scored based on two specific indicators, namely the time of flowering and the rosette leave number (RLN) at the time of bolting [37]. Under long-day (LD) photoperiod conditions, soil grown *aprf1-7* and *aprf1-9* mutant plants exhibited a delayed flowering time phenotype compared to WT. While the reproductive phase transition initiated in WT plants at *c.* 26 DAS with 12-13 RLN, *APRF1* impaired plants flowered at *c.* 34 DAS with 22-24 RLN (Fig. 4A, see also Fig. 5 D).

In addition to flowering time and RLN, another indicator of delayed flowering is the increased number of inflorescence internodes [37]. Under LD light conditions, WT plants normally acquire two to three inflorescence internodes (Fig. 4B and F). Remarkably, both *aprf1-7* and *aprf1-9* mutants developed inflorescences with an increased number of secondary branches. In *aprf1-7* the number of axillary buds varied from five to seven, while in the more severe *aprf1-9* phenotype up to nine paraclades were frequently observed (Fig. 4C–F). Not surprisingly, due to the enhanced and prolonged vegetative phase, several developmental morphometric parameters were also altered in the *APRF1* impaired plants. In WT, the average dry weight biomass was 180 ± 39 mg, whereas that of *aprf1-7* and *aprf1-9* mutant plants 250 ± 59 mg and 269 ± 46 mg, respectively. At full maturity, WT plants displayed an average height of *c.* 34 cm, whereas that of mutants were *c.* 42 cm (*aprf1-*

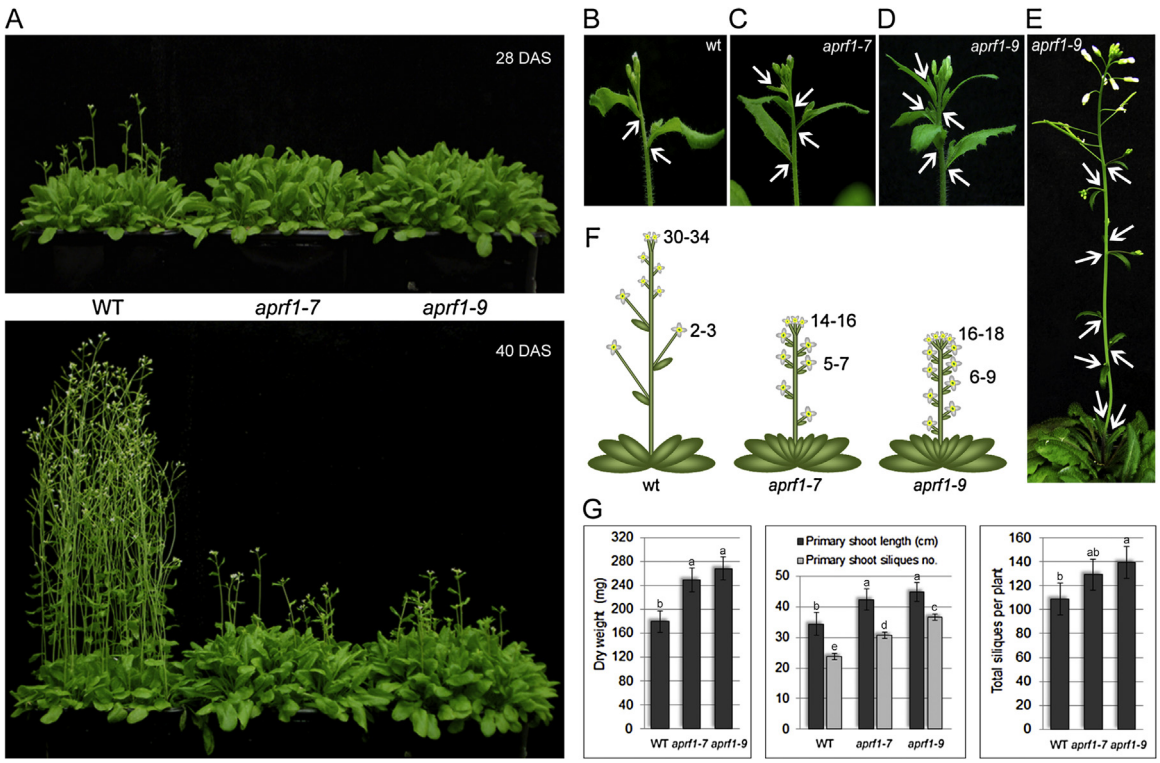

Fig. 4. Late flowering phenotypes of *aprf1-7* and *aprf1-9* mutants. (A) Images showing 28 DAS and 40 DAS WT and *aprf1* mutants growing on soil under LD photoperiod. (B–E) Primary inflorescence stems of a WT (B), *aprf1-7* (C) and *aprf1-9* plant (D) at bolting (38 DAS). Arrows indicate the increased number of axillary buds in mutants. At 48 DAS, up to nine paraclades were frequently observed in *aprf1-9* (E). (F) Schematic illustration of the mean phenotypes at 48 DAS, showing the number of flowers on the apical internodes and of secondary inflorescences. (G) Biometric analysis in WT and *aprf1* mutants. The graphs show measurements of dry weight, shoot length and number of siliques. Letters show significant differences ($P < 0.05$, Student's *t*-test). Error bars indicate S.D. ($n = 50$).

7) and *c.* 44 cm (*aprf1-9*). Finally, the number of siliques, either on the primary shoot or the total, was *c.* 20–60% higher in the *aprf1* mutants compared to that of WT plants (Fig. 4G).

In plants, all aerial organs (except cotyledons) are developed post-embryonically from the hemispherical self-sustaining SAM. Their formation is controlled by a highly organized pattern of cell division and expansion within the meristem [38]. In order to obtain a clearer picture regarding the consequences of *aprf1* mutation in meristem organization, semi-thin sections from shoot apices were examined. The analysis revealed that both the length of the SAM and the cell number of the L1 layer were affected in the mutants. WT plants had a meristem width of *c.* 76 μm, comprised by *c.* 16 cells. On the contrary, *aprf1-9* mutants displayed a slightly increased SAM width (83 μm), harboring *c.* 19 L1 layer cells (Fig. 5F, G). Interestingly, sections obtained from the apices of 24-DAS-old plants revealed that both WT and the mutant SAM displayed an architecture, characteristic of meristems that have undergone floral transition (Fig. 5H). Taken together, the above data suggest that the late flowering phenotype of *aprf1* mutants may rather be attributed to a delayed bolting than to a hindered floral transition.

3.5. Over-expression of APRF1 promotes flowering

In order to clarify how the developmental defects of both *aprf1* alleles are associated with the functional role of APRF1, we examined the consequences of a constitutive APRF1 expression. *APRF1* overexpression was evaluated in both Col-0 and *aprf1-9* genetic backgrounds by using a CaMV35S:*APRF1* construct (Supplementary Fig. A1). At least nine independent overexpressor lines from each genetic background and their segregating progeny were studied. The analysis showed that the transgenic lines displayed an early flowering phenotype, indicating not only the dominant effect of *APRF1* overexpression in WT, but also the functional complementation of the *aprf1* mutation (Fig. 5A, C). Lines displaying the most severe phenotype, were selected to obtain homozygous plants. *APRF1* transcript levels, as evaluated by qPCR at four time points, were substantially elevated in these overexpressors and ranged from 4- to 7-fold higher than in WT plants. On the contrary, *aprf1-9* mutants displayed negligible levels of *APRF1* transcripts (Fig. 5E). Offspring from lines 35S:*APRF1*[*aprf1-9*]-3 and 35S:*APRF1*[Col-0]-8, which showed the highest mRNA levels and the most prominent early flowering phenotype were used in all subsequent experiments.

The comparative analysis showed that *aprf1* mutants initiated flowering at 34 DAS (with *c.* 22-24 RLN). At the same time point, WT plants, which flowered eight days earlier (with *c.* 12-13 RLN), had several mature open flowers and three developed auxiliary buds on their primary inflorescence (Fig. 5A, B and D). On the contrary, the overexpression lines initiated flowering at 21 DAS, with an average RLN of 8.4 (Fig. 5D). Thus, 35S:*APRF1* plants displayed an early flowering phenotype compared with WT, possessing at 34 DAS multiple secondary inflorescences and fully developed siliques (Fig. 5C). Semi-thin sections of shoot apices showed that both the SAM width and the cell number were slightly decreased in the overexpression line. Compared to WT and the *APRF1* impaired plants, which displayed *c.* 16 and 19 L1 cells, respectively, the meristem of 35S:*APRF1* plants contained an average of 14 cells (Fig. 5F, G). Taken together, the above data suggest that the early flowering phenotype can be attributed to the increased *APRF1* transcript levels, which were also able to reverse the late flowering phenotype of *aprf1* mutants.

A further analysis was conducted, by measuring the time margins of specific developmental indicators (Fig. 5I) in the populations of the different genetic backgrounds (WT, *aprf1-9* and 35S:*APRF1*).

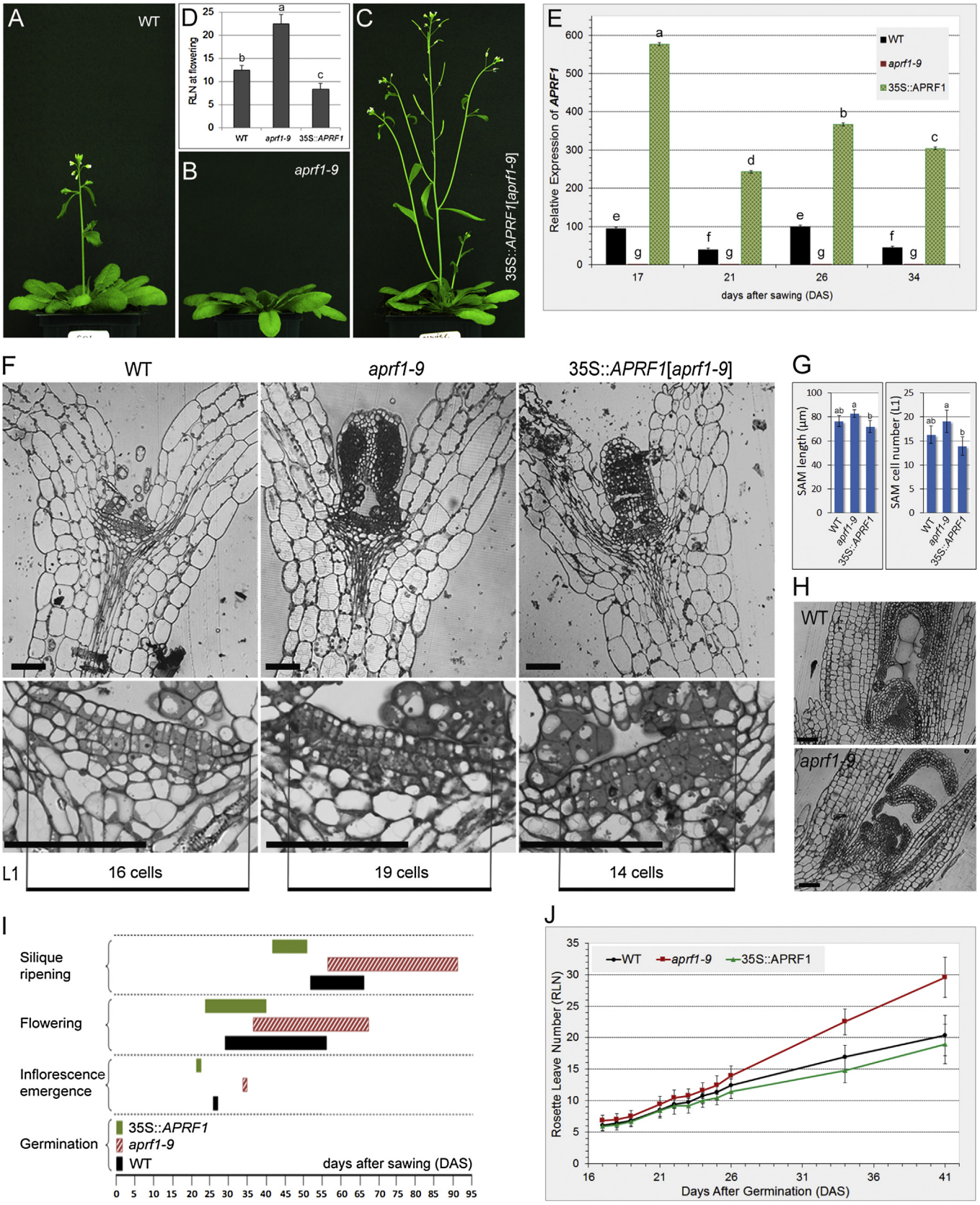

Fig. 5. Phenotypic and molecular analysis of *aprf1-9* mutants and *APRF1* overexpressors. (A) WT plant at 34 DAS with primary inflorescence and three auxiliary buds. (B) Image of an *aprf1-9* plant at 34 DAS, in the onset of bolting. (C) Image of an 35S:*APRF1*[*aprf1-9*] at 34 DAS. *APRF1* impaired plants were late flowering, while plants overexpressing *APRF1* displayed an early flowering phenotype. (D) Rosette leaf number at bolting of WT, *aprf1-9* and 35S:*APRF1*[*aprf1-9*] plants grown under LD conditions. (E) Relative expression of *APRF1* in the three genetic backgrounds, showing a 4 to 7-fold increase of transcripts in the overexpressors compared to WT. On the contrary, *APRF1* transcripts were undetectable in *aprf1-9* mutants. Letters show significant differences ($P < 0.05$, Student's *t*-test). Error bars indicate S.D. ($n = 4$). (F) Toluidine blue-stained longitudinal semi-thin sections of SAM from a representative WT, mutant and overexpressor plant (7 DAS).

As shown in Fig. 5I, the *APRF1* compromised plants displayed not only a delay in flowering, but also an extended flowering duration. The last developmental stage of silique ripening was also extended in mutant plants compared to WT by 25 days. Consequently, the life span of *aprf1* mutants was significantly prolonged to over 90 days compared to WT and 35S:*APRF1* plants, which were *c.* 65 and 47 days, respectively. However, seed germination time margins were unaffected in the three genetic backgrounds, suggesting that the observed phenotypic differences were not caused by an alteration in germination time (Fig. 5I). The number of rosette leaves, either juvenile or adult, depends on both the duration of the vegetative phase and the rate of leaf production [39]. As demonstrated in Fig. 5J, the rate of leaf production was increased in the *aprf1* mutants, leading at day 42 to a higher number of RLN compared to WT. On the contrary, the corresponding rate was decreased in the overexpression lines, resulting in plants with less RLN than in WT (Fig. 5J).

3.6. APRF1 is localized in the nucleus

To obtain insights into the subcellular distribution of the APRF1 protein, a *YFP:APRF*1 translational fusion construct was generated (Supplementary Fig. A1). Agrobacterium-mediated transformation was used to obtain stable transgenic *Arabidopsis* plants, as well as transiently transformed *N. benthamiana* leaf cells. The analysis revealed that APRF1 is a nuclear protein, as evidenced by the strong fluorescent YFP signal emitted from the nucleoplasm of *Arabidopsis* root cells and differentiated tobacco epidermal cells. Noteworthy, the signal did not mark the nucleolar region of the nuclei (Fig. 6), indicating that APRF1 is not involved in the functional steps necessary for synthesis and assembly of preribosomal particles.

3.7. APRF1 functionally complements S. cerevisiae swd2 mutant

The yeast Swd2 is an essential subunit for the CPF complex, necessary for mRNA 3′ processing, as well as for the COMPASS complex, involved in H3K4 histone methylation [6]. As APRF1 shows significant sequence and structural homology to Swd2 (Supplementary Fig. A3), the functional conservation between the two orthologs was investigated. Yeast strain Y40075 contains a heat inducible degron cassette at the YKL018 w ORF (Swd2), the activation of which results in growth arrest upon shifting cells to non-permissive temperatures. To examine the functional complementation of the yeast mutant by APRF1, two distinct constructs were assessed (Supplementary Fig. A2). As shown in Fig. 7A and B, yeast cells transformed with either the p416APRF1a or p416APRF1b construct, or with the empty p416GPD vector alone, displayed normal growth on glucose-containing media plates both at 25 °C and 37 °C (UBR1 OFF). Upon activation of UBR1 gene by galactose (UBR1 ON), the growth of the degron strain cells containing the empty vector was arrested at 37 °C (Fig. 7D). To the contrary, yeast cells expressing APRF1 were able to grow under this non-permissive temperature, indicating a functional complementation of the degron strain by the *A. thaliana* APRF1 protein (Fig. 7D).

3.8. APRF1 acts upstream of FLC

Flowering time control is regulated by a large number of genes, which act in several overlapping pathways to induce and initiate the plant reproductive phase under different environmental conditions. The expression of many of these flowering genes, including the key regulator *FLC*, is modulated through histone modifications [40,41]. Considering the late flowering phenotype of *aprf1* and the functional homology of APRF1 with the yeast Swd2 subunit of the COMPASS histone methylation complex, we investigated the possibility whether the observed phenotypes were caused by misregulation of the flowering time loci. Therefore, qPCR was employed to evaluate the expression levels of the major flowering time genes *FLC*, *SOC1*, *CO* and *FT*, in WT and *aprf1* plants under LD (Fig. 8). The analysis revealed that *FLC* transcript levels were extremely elevated in mutant plants at all time points. At 21 DAS, when the plants were still in the vegetative phase, *aprf1* displayed a 14-fold increase in *FLC* mRNA levels compared to WT. Even though *FLC* expression was significantly reduced in mutants at 26 DAS and 34 DAS, their transcript levels were still higher than in WT plants by 21-fold and 32-fold, respectively (Fig. 8B). These results support the view that flowering of *aprf1* was hindered by the elevated expression of *FLC* and that *APRF1* is probably involved in an *FLC* downregulation mechanism to accelerate flowering under LD conditions. Consistent with the late flowering phenotype of *aprf1* plants and the elevated *FLC* transcripts, expression of *CO* and *SOC1* was significantly reduced in the mutants at 21 and 26 DAS. However, their transcription raised at 34 DAS, the time point of *aprf1* bolting. *CO* in particular, displayed a drastic 4-fold increase in gene expression compared to WT (Fig. 8C and D), while *FT* transcripts were found to be slightly elevated at all time points (Fig. 8E).

4. Discussion

Plant development depends largely on the proper assembly of protein complexes and their cooperative action within complicated regulatory networks. Here, we report on the characterization of the WD40 scaffolding protein APRF1, which participates most likely in complexes that ensure normal meristem activity and promote flowering in *Arabidopsis* under LD photoperiod.

Phylogenetic clustering of APRF1 from *Arabidopsis* and other eukaryotes depicted the conserved WD40 motif within these proteins. Unlike other eukaryotes, plants contain two closely related homologs in their genome, denoting the occurrence of a gene-duplication event before the divergence of the plant lineage [42]. In *Arabidopsis*, the homolog of *APRF1* encodes for the previously characterized ULCS1 protein [34]. Although homologous, APRF1 and ULCS1 proteins appear to have distinct functions. ULCS1 has been characterized as a putative subunit of a DWD Cul4-RING E3 ligase complex, involved in the regulation of secondary wall modifications. On the other hand, APRF1 displays a functional homology to the yeast Swd2 protein, a subunit both of COMPASS and CPF complexes (present study). The ability of the *Arabidopsis* APRF1 protein to rescue the yeast *swd2Δ* phenotype indicates its possible recruitment, similarly to yeast, in the assembly of analogous complexes. Thus, it is tempting to speculate that APRF1 may be a component of two distinct molecular functions, histone methylation and RNAP II transcription termination and 3′ end processing. This hypothesis could also be corroborated by the exclusive nuclear localization of APRF1. In plants, a similar dual function has been reported for FCA and FPA, which are known as repressors of the flowering time regulator *FLC*. Although their function has been associated with chromatin modifications at several loci, including *FLC*, they also

The length of the L1 layer and the number of L1 cells are indicated. The meristem of *aprf1-9* contained fewer cells, while that of the overexpressor more and smaller cells. Bars: 50 μm. (G) Graphical representation of average SAM length and cell number. Letters show significant differences ($P < 0.05$, Student's *t*-test). Error bars indicate S.D. ($n = 5$). (H) Toluidine blue-stained longitudinal semi-thin sections of SAM from a representative WT and *aprf1-9* mutant plant at 24 DAS. (I) Schematic representation of the chronological progression of specific growth stages in WT, *aprf1-9* and 35S:*APRF1*[*aprf1-9*] plant populations ($n = 50$). (J) Graph showing the production of rosette leaves (RLN) over time in WT, *aprf1-9* and 35S:*APRF1*[*aprf1-9*] plant populations. Note the increased RLN rate of *aprf1-9* compared to WT and the *APRF1* overexpressor. Error bars indicate S.D. ($n = 50$).

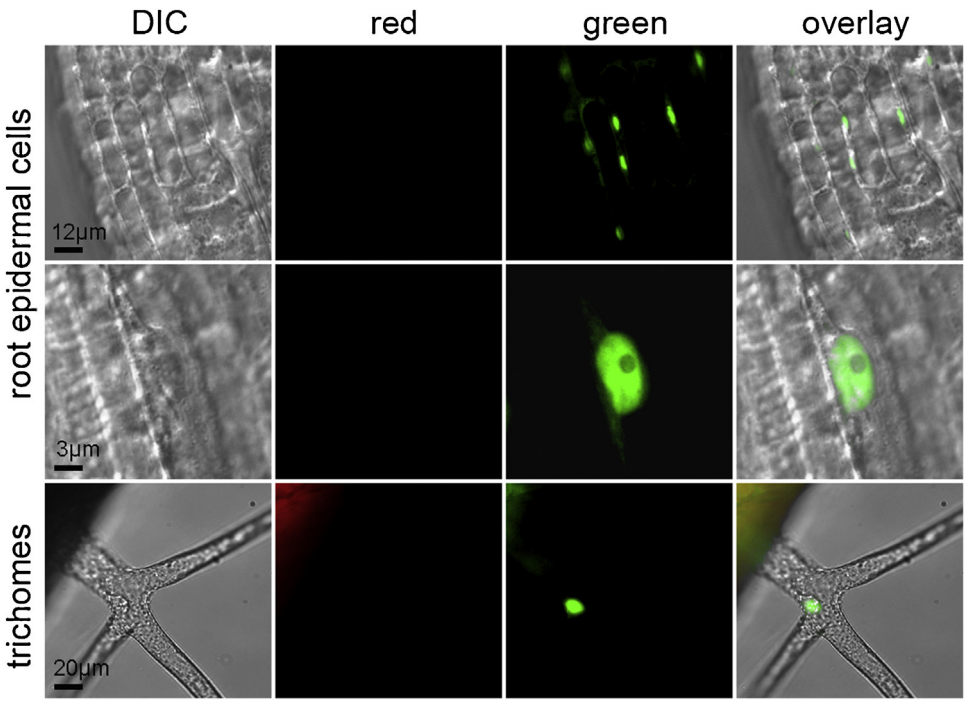

Fig. 6. Subcellular localization of APRF1 *in planta*. Images showing the distribution of the chimeric *YFP:APRF1* fusion protein in root epidermal cells and trichomes of transgenic *A. thaliana* plants. APRF1 was predominantly localized in the nucleoplasm and was absent from the nucleolus. DIC, Differential Interference Contrast images; red, autofluorescence of chlorophyll; green, images with GFP filters; overlay, GFP images superimposed on DIC images. (For interpretation of the references to colour in this figure legend, the reader is referred to the web version of this article.)

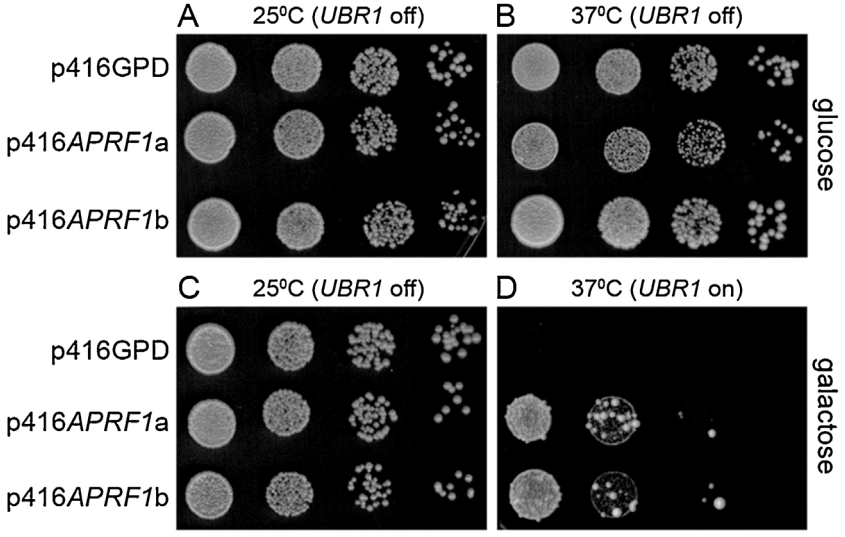

Fig. 7. Functional conservation between APRF1 and Swd2. Serial dilutions of yeast degron strain cells (Y40075), harboring the p416APRF1a or p416APRF1b expression construct, or the empty vector were spotted on plates containing glucose (A, B) or galactose (C, D) and incubated at permissive (25 °C) or non-permissive (37 °C) temperatures for 48–72 h. Yeast cells plated on SC Glu either at 25 °C or 37 °C (UBR1 OFF) and SC Gal at 25 °C (UBR1 OFF) exhibited normal growth. On SC Gal plates at 37 °C (UBR1 ON) the growth of the Y40075 degron strain cells containing the empty vector was arrested. To the contrary, yeast cells expressing *APRF1* were able to grow under this non-permissive temperature, indicating functional complementation of the degron strain by the *A. thaliana* APRF1 protein.

play important roles in genome-wide RNA 3′ processing and transcription termination [43].

In LD, *APRF1*-impaired plants displayed a delayed bolting and consequently a late flowering phenotype, with an average of 10 additional rosette leaves compared to WT. This delayed flowering led to additional alterations during development. The extended vegetative growth phase resulted in larger rosette leaves, which were more elongated with extended petioles and an undulating surface. Overall, the phenotype of *aprf1* resembled that of WT plants grown under SD photoperiod [36,44]. However, *aprf1* plants exhibited at the same time an unaccustomed increased growth rate. Meristem activity was enhanced during the vegetative phase, thus allowing the development of multiple inflorescence primordia. This was evident during bolting by the emergence and establishment of up to 9 branches on the primary shoot of each plant. Although the number of bracts produced in the inflorescence is dependent on the duration of the early inflorescence phase [44], *aprf1-9* mutants developed significantly more bracts than WT plants grown under SD. When a *35S:APRF1* construct was introduced into *aprf1-9* mutants, their late flowering phenotype was reversed to early

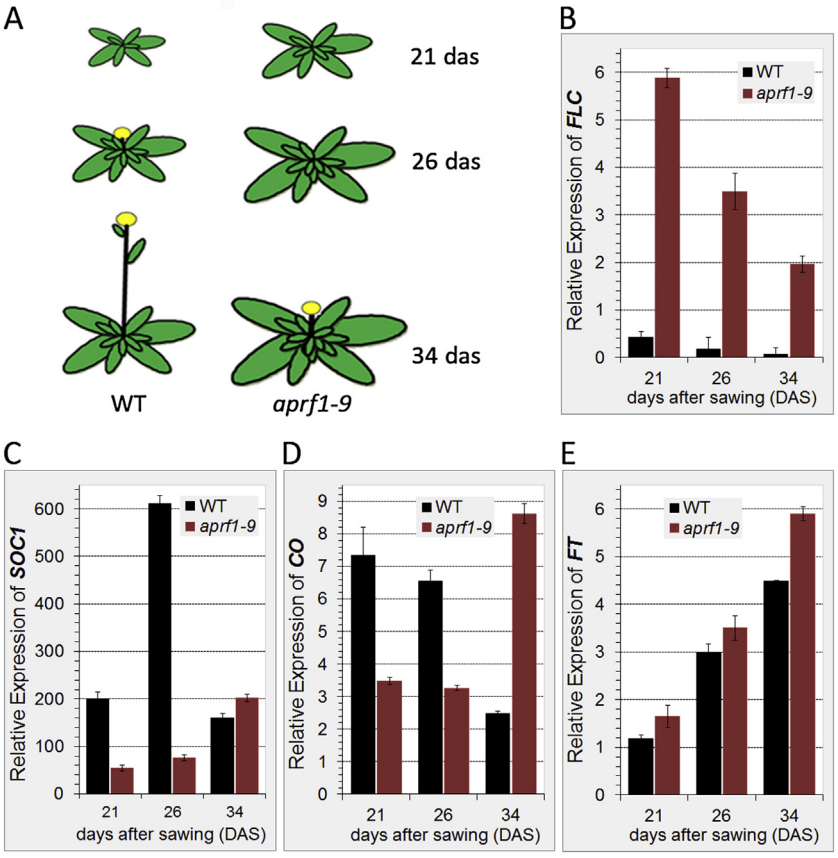

Fig. 8. Relative expression of key flowering genes. (A) Schematic representation of the mean phenotype of WT and *aprf1-9* plants at 21 DAS (vegetative phase), 26 DAS (the time of WT flowering) and 34 DAS (the time of *aprf1-9* flowering). (B–E) Quantitative RT-PCR analysis showing the relative expression of *FLC, SOC1, CO* and *FT* in WT plants and *aprf1-9* mutants. Values ± SD were normalized to *GAPDH* and represent the mean of three biological samples analyzed in triplicates.

flowering, not only in terms of timing, but also in terms of developmental deviations, such as SAM organization, RLN, number of internodes, biomass and length of primary shoot. However, time margins of seed germination were unaffected, indicating that the lateness in the initiation of flowering was due to the extension of the vegetative phase and not to an alteration of the germination time. The above data suggest that the overall phenotype of *aprf1* plants could be interpreted as the outcome of an elongated vegetative phase combined with the simultaneous increase of leaf and bract initiation rate. Thus, *APRF1* appear to be essential both for the normal meristem activity and for the establishment of the canonical floral developmental program.

Several reports have shown that various *Arabidopsis* genes encoding for WDR proteins in plants regulate diverse developmental processes, including flowering, through their involvement in E3 ligase or chromatin modification complexes [17,45]. For instance, *dcaf1cs* mutants, which are unable to form a functional ubiquitin ligase complex, exhibit atypical phyllotaxy and several inflorescence architecture abnormalities [46]. Downregulation of *ULCS1*, a putative subunit of an E3 DWD CRL complex causes pleiotropic phenotypes, including sterility and increased growth [34]. On the other hand, VERNALIZATION INDEPENDENT 3 (VIP3) forms in association with DAMAGE SPECIFIC DNA BINDING PROTEIN 1 (DDB1), an E3 DWD CRL that controls ubiquitin-mediated degradation of specific target proteins. Loss of VIP3 function leads to a redistribution of H3K4me3 and H3K36me2 modifications, resulting in pleiotropic phenotypes such as stunted growth, small rosette leaves and early flowering [47,48]. MSI4 (MULTICOPY SUPPRESSOR OF IRA1 4) also regulates flowering time in *Arabidopsis* epigenetically, via the interaction with a CUL4-DDB1 and a Polycomb Repressive Complex (PRC). Since CUL4 interacts with *FLC* chromatin in an MSI4-dependant manner, mutations in the *MSI4* locus reduces *FLC* H3K27 trimethylation, resulting in increased *FLC* expression and thus to a late flowering phenotype [46,49]. Similarly, the *Arabidopsis* MSI1 (MULTICOPY SUPPRESSOR OF IRA1) ortholog of Drosophilla p55, was found to bridge the LIKE HETEROCHROMATIN PROTEIN 1 (LHP1) with the PRC to re-establish reduced H3K27me3 levels to target sites [50]. However, MSI1 interact also with a CUL4-DDB1 complex and the RETINOBLASTOMA-RELATED (RBR) protein to control chromatin assembly [51], imprinting and gene expression in *Arabidopsis* [52,53]. As a histone binding protein, MSI1 also controls indirectly the transcript levels of *SOC1*, through the regulation of *CO* expression in the photoperiod pathway [54].

Given the functional homology between APRF1 and the yeast Swd2 protein, as well as the mutant and overexpression phenotypes, APRF1 may act in an analogous way. In consistence with the late flowering phenotype, *FLC* was found to be highly upregulated in *aprf1* plants. Although *FLC* expression dropped significantly during the prolonged vegetative phase, its transcripts remain considerably higher than in WT even at 34 DAS. In line to the above, expression of *CO* and *SOC1* was reduced in the mutants at 21 and 26 DAS. Nevertheless, while possibly delayed by the elevated *FLC* mRNA levels, *SOC1* expression displayed a gradual increase during the vegetative phase. At 34 DAS, transcript levels of both genes were higher in *aprf1* compared to WT plants, consistent with the onset of bolting observed at this time point. Furthermore, *FT* transcription was slightly elevated during all phases of vegetative development, suggesting that despite the increased *FLC*, *FT* expression was not

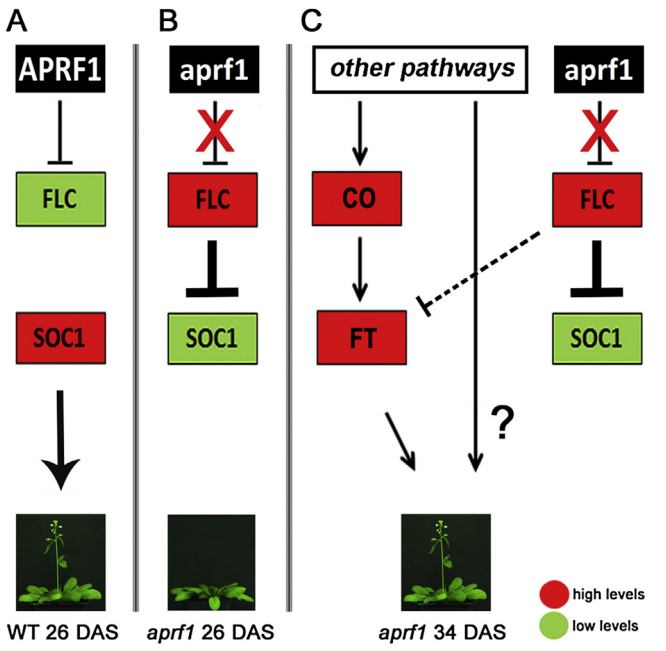

Fig. 9. Simplified schematic illustration of the proposed working model for *APRF1*. As a component of a hypothetical regulatory complex, *APRF1* may act upstream of *FLC* to suppress its expression. Low *FLC* and high *SOC1* transcripts stimulate the plant to flower at 26 DAS (A). In the absence of APRF1, the regulatory complex may not be assembled, leading to substantially higher *FLC* transcripts levels and, in turn, to the inability of the plants to flower on time. At 34 DAS, alternative flowering pathways or mechanisms may be activated to assist *aprf1* plants in entering the reproductive phase under LD (C).

suppressed. This is in accordance with previous reports showing that *FLC* expression in the meristem may delay flowering, but does not reduce *FT* mRNA levels in leaves [20,55]. Thus, the anticipated *FLC*-mediated inhibition of bolting in *aprf1*, may be circumvented through the activation of alternative floral-promotion pathways. This is in agreement with the widely accepted view that apart from *FLC* transcript levels, additional safeguard routes and mechanisms may be stimulated that ensure flowering. These could involve age-dependent mechanisms, ambient temperature, micro RNAs, SQUAMOSA-PROMOTER BINDING PROTEIN-LIKE (SPL) and DELLA proteins [22,23,56–61]. Based on our data, a simplified hypothetical model can be depicted to illustrate the putative role of *APRF1* during flowering (Fig. 9). According to this, APRF1 could be a subunit of a chromatin modification complex that promotes flowering in WT by suppressing *FLC* expression. Low *FLC* and high *CO* and *SOC1* transcripts lead, at 26 DAS, to the transition of the plants from the vegetative to the reproductive phase (Fig. 9A). In the *APRF1*-impaired plants, inhibition of *FLC* expression is not accomplished, resulting in reduced *SOC1* transcripts at this time point, which in combination with low *CO* levels rivet the plants in the vegetative phase for more than a week (Fig. 9B). Interestingly, meristem activity is not inhibited, since plants continue to produce secondary inflorescences that do not elongate. As development proceeds, alternative floral-induction pathways may be activated, to assist *aprf1* plants in overcoming the inhibitory effect of *FLC* and initiate bolting (Fig. 9C). However, it is unclear whether APRF1 interferes in FLC expression in a direct or indirect manner. Furthermore, due to the propeller-like structure of the WD40-domain, the involvement of APRF1 in the assembly of diverse complexes that regulate various target genes cannot be excluded.

In conclusion, our data underline the important role of APRF1 in *Arabidopsis* vegetative and reproductive development under LD. Its putative involvement in chromatin modification complexes may directly or indirectly influence the expression of key genes that regulate meristem activity and flowering time in *Arabidopsis*. Further approaches are needed, to identify both the interacting partners of APRF1 complexes and their putative targets. A comparative phenotypic and molecular analysis of mutant and overexpression lines under LD and SD, could also clarify its role in promoting flowering and elucidate the cross-talk of the multiple floral inductive pathways.

Conflict of interest

The authors declare that the research was conducted in the absence of any commercial or financial relationships that could be construed as a potential conflict of interest.

Acknowledgements

This work was supported by the European Social Fund and National Resources (EPEAK II) PYTHAGORAS and the NKUA Special Account For Research Grants (S.A.R.G.). We thank the Salk Institute and the NASC for providing the *Arabidopsis* T-DNA insertion lines and Stamatis Rigas for critical reading the manuscript. The authors also wish to apologize to those authors whose excellent work could not be cited due to space restrictions.

Appendix A. Supplementary data

Supplementary data associated with this article can be found, in the online version, at http://dx.doi.org/10.1016/j.plantsci.2016.09.015.

References

[1] L. Yu, C. Gaitatzes, E. Neer, T.F. Smith, Thirty-plus functional families from a single motif, Protein Sci. 9 (2000) 2470–2476.
[2] S. van Nocker, P. Ludwig, The WD-repeat protein superfamily in Arabidopsis: conservation and divergence in structure and function, BMC Genomics 4 (2003) 50.
[3] C.U. Stirnimann, E. Petsalaki, R.B. Russell, C.W. Müller, WD40 proteins propel cellular networks, Trends Biochem. Sci. 35 (2010) 565–574.
[4] T.F. Smith, C. Gaitatzes, K. Saxena, E.J. Neer, The WD repeat: a common architecture for diverse functions, Trends Biochem. Sci. 24 (1999) 181–185.
[5] T.F. Smith, TF, Diversity of WD-Repeat Proteins, in: C.S. Clemen, L. Eichinger, V. Rybakin (Eds.) The coronin family of proteins, Subcellular biochemistry, (2008) pp. 20–30.
[6] H. Cheng, X. He, C. Moore, The essential WD repeat protein Swd2 has dual functions in RNA polymerase II transcription termination and lysine 4 methylation of histone H3, Mol. Cell. Biol. 24 (2004) 2932–2943.
[7] B. Dichtl, R. Aasland, W. Keller, Functions for *S. cerevisiae* Swd2p in 3- end formation of specific mRNAs and snoRNAs and global histone 3 lysine 4 methylation, RNA 10 (2004) 965–977.
[8] L.M. Soares, S. Buratowski, Yeast swd2 is essential because of antagonism between set1 histone methyltransferase complex and APT (Associated with pta1) termination factor, J. Biol. Chem. 287 (2012) 15219–15231.
[9] C. Xu, J. Min, Structure and function of WD40 domain proteins, Protein Cell 2 (2011) 202–214.
[10] C. Zhang, F. Zhang, The multifunctions of WD40 proteins in genome integrity and cell cycle progression, J. Genomics 3 (2015) 40–50.
[11] Q. Li, P. Zhao, J. Li, C. Zhang, L. Wang, Z. Ren, Genome-wide analysis of the WD-repeat protein family in cucumber and Arabidopsis, Mol. Genet. Genomics 289 (2014) 103–124.
[12] W. Wang, Q. Zhang, D. Guo, An *Artemisia* WD40-Repeat gene regulates multiple cellular functions in Arabidopsis, J.Biosci. Med. 4 (2016) 30–36.
[13] N. Xu, X.Q. Gao, X.Y. Zhao, D.Z. Zhu, L.Z. Zhou, X.S. Zhang, Arabidopsis *AtVPS15* is essential for pollen development and germination through modulating phosphatidylinositol 3-phosphate formation, Plant Mol. Biol. 77 (2011) 251–260.
[14] K.N. Bjerkan, S. Jung-Romeo, G. Jurgens, P. Genschik, P.E. Grini, Arabidopsis WD REPEAT DOMAIN55 interacts with DNA DAMAGED BINDING PROTEIN1 and is required for apical patterning in the embryo, Plant Cell 24 (2012) 1013–1033.
[15] H. Kaya, K. Shibahara, K. Taoka, M. Iwabuchi, B. Stillman, T. Araki, *FASCIATA* genes for chromatin assembly factor-1 in Arabidopsis maintain the cellular organization of apical meristems, Cell 104 (2001) 131–142.
[16] H. Onouchi, M.I. Igeno, C. Perilleux, K. Graves, G. Coupland, Mutagenesis of plants overexpressing *CONSTANS* demonstrates novel interactions among Arabidopsis flowering-time genes, Plant Cell 12 (2000) 885–900.

[17] D.H. Jiang, N.C. Kong, X.F. Gu, Z.C. Li, Y.H. He, Arabidopsis COMPASS-like complexes mediate histone H3 lysine-4 trimethylation to control floral transition and plant development, PLoS Gen. 7 (2011) e1001330.
[18] F. Turck, F. Fornara, G. Coupland, Regulation and identity of florigen: FLOWERING LOCUS t moves center stage, Ann. Rev. Plant Biol. 59 (2008) 573–594.
[19] J. Moon, S.S. Suh, H. Lee, K.R. Choi, C.B. Hong, N.C. Paek, S.G. Kim, I. Lee, The *SOC1* MADS-box gene integrates vernalization and gibberellins signals for flowering in Arabidopsis, Plant J. 35 (2003) 613–623.
[20] X. Hou, J. Zhou, C. Liu, L. Liu, L. Shen, H. Yu, Nuclear factor Y-mediated H3K27me3 demethylation of the *SOC1* locus orchestrates flowering responses of Arabidopsis, Nat. Commmun. (2014), http://dx.doi.org/10.1038/ncomms5601.
[21] R.N. Wilson, J.W. Heckman, C.R. Somerville, Gibberellin is required for flowering in *Arabidopsis thaliana* under short days, Plant Physiol. 100 (1992) 403–408.
[22] A. Srikanth, M. Schmid, Regulation of flowering time: all roads lead to Rome, Cell. Mol. Life Sci. 68 (2011) 2013–2037.
[23] J. Lee, I. Lee, Regulation and function of SOC1, a flowering pathway integrator, J. Exp. Bot. 61 (2010) 2247–2254.
[24] S. Berry, C. Dean, Environmental perception and epigenetic memory: mechanistic insight through *FLC*, Plant J. 83 (2015) 133–148.
[25] Y.Y. Levy, S. Mesnage, J.S. Mylne, A.R. Gendall, C. Dean, Multiple roles of arabidopsis VRN1 in vernalization and flowering time control, Science 297 (2002) 243–246.
[26] S.D. Michaels, R.M. Amasino, *FLOWERING LOCUS C* encodes a novel MADS domain protein that acts as a repressor of flowering, Plant Cell 11 (1999) 949–956.
[27] C.C. Sheldon, D.T. Rouse, E.J. Finnegan, W.J. Peacock, E.S. Dennis, The molecular basis of vernalization: the central role of FLOWERING LOCUS C (FLC), PNAS 97 (2000) 3753–3758.
[28] H. Lee, S.S. Suh, E. Park, E. Cho, J.H. Ahn, S.G. Kim, J.S. Lee, Y.M. Kwon, I. Lee, The AGAMOUS-LIKE 20 MADS domain protein integrates floral inductive pathways in Arabidopsis, Genes Dev. 14 (2000) 2366–2376.
[29] G.G. Simpson, C. Dean, Arabidopsis, the Rosetta stone of flowering time? Science 296 (2002) 285–289.
[30] Y. Komeda, Genetic regulation of time to flower in *Arabidopsis thaliana*, Ann. Rev. Plant Biol. 55 (2004) 521–535.
[31] A. Pajoro, S. Biewers, E. Dougali, F.L. Valentim, M.A. Mendes, A. Porri, G. Coupland, Y. van de Peer, A.D.J. van Dijk, L. Colombo, B. Davies, G.C. Angenent, The (r)evolution of gene regulatory networks controlling Arabidopsis plant reproduction: a two-decade history, J. Exp. Bot. 65 (2014) 4731–4745.
[32] Y. Wang, X.J. Hu, X.D. Zou, X.H. Wu, Z.Q. Ye, Y.D. Wu, WDSPdb: a database for WD40-repeat proteins, Nucleic Acids Res. 43 (2014) 339–344, http://dx.doi.org/10.1093/nar/gku1023.
[33] A. Sanchez-Diaz, M. Kanemaki, V. Marchesi, K. Labib, Rapid depletion of budding yeast proteins by fusion to a heat-inducible degron, Science's STKE 2004 (2004) pl8.
[34] D. Beris, G. Kapolas, P. Livanos, A. Roussis, D. Milioni, K. Haralampidis, RNAi-mediated silencing of the *Arabidopsis thaliana ULCS1* gene, encoding a WDR protein, results in cell wall modification impairment and plant infertility, Plant Sci. 245 (2016) 71–83.
[35] S. Pouteau, C. Albertin, The significance of bolting and floral transitions as indicators of reproductive phase change in Arabidopsis, J. Exp. Bot. 60 (2009) 3367–3377.
[36] J. Clarke, D. Tack, K. Findlay, M. van Montagu, M. van Lijsebettens, The *SERRATE* locus controls the formation of the early juvenile leaves and phase length in Arabidopsis, Plant J. 20 (1999) 493–501.
[37] S. Pouteau, C. Albertin, An assessment of morphogenetic fluctuation during reproductive phase change in Arabidopsis, Ann. Bot. 107 (2011) 1017–1027.
[38] R.S. Poethig, Phase change and the regulation of developmental timing in plants, Science 301 (2003) 334–336.
[39] A. Telfer, K.M. Bollman, R.S. Poethig, Phase change and the regulation of trichome distribution in *Arabidopsis thaliana*, Development 124 (1997) 645–654.
[40] P. Crevillen, C. Dean, Regulation of the floral repressor gene *FLC*: the complexity of transcription in a chromatin context, Curr. Opin. Plant Biol. 14 (2011) 38–44.
[41] Y. He, Chromatin regulation of flowering, Trends Plant Sci. 17 (2012) 556–562.
[42] N.D. Pires, L. Dolan, Morphological evolution in land plants: new designs with old genes, Philos. Trans. R. Soc. B 367 (2012) 508–518.
[43] C. Sonmez, I. Bäurle, A. Magusin, R. Dreos, S. Laubinger, D. Weigel, C. Dean, RNA 3′ processing functions of Arabidopsis FCA and FPA limit intergenic transcription, PNAS 108 (2011) 8508–8513.
[44] O.J. Ratcliffe, I. Amaya, C. Vincent, S. Rothstein, R. Carpenter, E.S. Coen, D.J. Bradley, A common mechanism controls the life cycle and architecture of plants, Development 125 (1998) 1609–1615.
[45] J.R. Wilson, N. Justin, Histone recognition by WD40 proteins, in: M.M. Zhou (Ed.), Histone Recognition, Springer International Publishing, Switzerland, 2015, pp. 83–100.
[46] Y. Zhang, S. Feng, F. Chen, H. Chen, J. Wang, C. McCall, Y. Xiong, X.W. Deng, Arabidopsis DDB1-CUL4 ASSOCIATED FACTOR1 forms a nuclear E3 Ubiquitin Ligase with DDB1 and CUL4 that is involved in multiple plant developmental processes, Plant Cell 20 (2008) 1437–1455.
[47] H. Zhang, C. Ransom, P. Ludwig, S. van Nocker, Genetic analysis of early flowering mutants in Arabidopsis defines a class of pleiotropic developmental regulator required for expression of the flowering-time switch *Flowering Locus C*, Genetics 164 (2003) 347–358.
[48] J.H. Lee, W. Terzaghi, G. Gusmaroli, J.B.F. Charron, H.J. Yoon, H. Chen, Y.J. He, Y. Xiong, X.W. Deng, Characterization of arabidopsis and rice DWD proteins and their roles as substrate receptors for CUL4-RING E3 ubiquitin ligases, Plant Cell 20 (2008) 152–157.
[49] M. Pazhouhandeh, J. Molinier, A. Berr, P. Genschik, MSI4/FVE interacts with CUL4–DDB1 and a PRC2-like complex to control epigenetic regulation of flowering time in Arabidopsis, PNAS 108 (2011) 3430–3435.
[50] M. Derkacheva, Y. Steinbach, T. Wildhaber, I. Mozgova, W. Mahrez, P. Nanni, S. Bischof, W. Gruissem, L. Hennig, Arabidopsis MSI1 connects LHP1 to PRC2 complexes, EMBO J. 32 (2013) 2073–2085.
[51] L. Hennig, R. Bouveret, W. Gruissem, MSI1-like proteins: an escort service for chromatin assembly and remodeling complexes, Trends Cell Biol. 15 (2005) 295–302.
[52] P.E. Jullien, A. Mosquna, M. Ingouff, T. Sakata, N. Ohad, F. Berger, Retinoblastoma and its binding partner MSI1 control imprinting in Arabidopsis, PLOS 6 (2008) e194.
[53] E. Dumbliauskas, E. Lechner, M. Jaciubek, A. Berr, M. Pazhouhandeh, V. Alioua, V. Brukhin, C. Koncz, U. Grossniklaus, J. Molinier, P. Genschik, The Arabidopsis CUL4–DDB1 complex interacts with MSI1 and is required to maintain MEDEA parental imprinting, EMBO J. 30 (2011) 731–743.
[54] Y. Steinbach, L. Hennig, Arabidopsis MSI1 functions in photoperiodic flowering time control, Front. Plant Sci. (2014), http://dx.doi.org/10.3389/fpls.2014.00077.
[55] I. Searle, Y. He, F. Turck, C. Vincent, F. Fornara, S. Kröber, R.A. Amasino, G. Coupland, The transcription factor FLC confers a flowering response to vernalization by repressing meristem competence and systemic signaling in Arabidopsis, Genes Dev. 20 (2006) 898–912.
[56] P. Huijser, M. Schmid, The control of developmental phase transitions in plants, Development 138 (2011) 4117–4129.
[57] A. Yamaguchi, M. Abe, Regulation of reproductive development by non-coding RNA in Arabidopsis: to flower or not to flower, Curr. Top. Plant Res. 125 (2012) 693–704.
[58] R.S. Poethig, Vegetative phase change and shoot maturation in plants, Curr. Top. Dev. Biol. 105 (2013) 125–152.
[59] U. Lutz, D. Posé, M. Pfeifer, H. Gundlach, J. Hagmann, C. Wang, D. Weigel, K.F.X. Mayer, M. Schmid, C. Schwechheimer, Modulation of ambient temperature-dependent flowering in *Arabidopsis thaliana* by natural variation of *FLOWERING LOCUS M*, PLOS Gen (2015), http://dx.doi.org/10.1371/journal.pgen.1005588.
[60] Y. Hyun, R. Richter, C. Vincent, R. Martinez-Gallegos, A. Porri, G. Coupland, Multi-layered regulation of SPL15 and cooperation with SOC1 integrate endogenous flowering pathways at the Arabidopsis shoot meristem, Dev. Cell 37 (2016) 254–256.
[61] M. Li, F. An, W. Li, M. Ma, Y. Feng, X. Zhang, H. Guo, DELLA proteins interact with FLC to repress flowering transition, J. Integr. Plant Biol. 58 (2016) 642–655.